MRS Communications (2015), 5, 243–250

doi:10.1557/mrc.2015.31

MRS Communications

Polymers/Soft Matter Research Letter

Real-time imaging of chromophore alignment in photorefractive polymer devices through multiphoton microscopy

Brittany Lynn, Alexander Miles, Soroush Mehravar, Pierre-Alexandre Blanche, Khanh Kieu, Robert A. Norwood, and **N. Peyghambarian,** College of Optical Sciences, The University of Arizona, Tucson, Arizona, USA

Address all correspondence to Pierre-Alexandre Blanche at **pablanche@optics.arizona.edu**

(Received 28 January 2015; accepted 29 April 2015)

Abstract

A model with which to predict the effect of coplanar electrode geometry on diffraction uniformity in photorefractive polymer display devices was developed. Assumptions made in the standard use cases are no longer valid in the regions of extreme electric fields present in this type of device. Using electric-field induced second-harmonic generation through multiphoton microscopy, the physical response in regions of internal electric fields which fall outside the standard regimes of validity were probed. Adjustments to the standard model were made and the results of the new model corroborated through holographic four-wave mixing measurements.

Introduction

The photorefractive (PR) effect in organic polymeric systems has been under investigation for more than 25 years and has been driven recently by its use as recording media in updatable holography based three-dimensional (3D) displays.[1] As a dynamic holographic recording media, PR polymers are attractive due to their lack of any post-illumination processing requirements and the ability to erase and record a new hologram at will. These devices exhibit sub-micron fringe resolution, recording/rewriting times in the milliseconds, and diffraction efficiencies of 100%.[2,3] Standard polymeric processing techniques have facilitated the development of display devices larger than 900 cm^2.[4]

In this type of display system, two coherent beams are used to record the image, one holding the scene information, called the object beam, and the other acting as a reference beam. When these two beams overlap in the material, they create an interference pattern that encodes the information from both wavefronts. The PR polymer in this study is composed of four main components which together allow it to record this intensity variation: a hole-conducting polymer polyacrylic-tetraphenyldiaminobiphenyl (PATPD), the plasticizer ethyl carbazole (ECZ), 4-homopiperidino benzylidine-malonitrile (7-DCST) chromphore, and a sensitizer [6,6]-phenyl-C61-butyric acid methyl ester (PCMB) in a ratio of 51.5:20:28:0.5 wt%, respectively. Upon illumination, excitons are created on the PCBM due to photon absorption in the regions of constructive interference. Upon separation under an externally applied electric field (E^0), the holes drift through the film along the PATPD until they become trapped in the dark regions of the fringes. This separation of charges creates a space-charge field (E_{sc}) that mimics the incident fringes and aligns the chromophores, leading to a spatial variation of the index of refraction (Δn). The presence of ECZ reduces the glass transition temperature of the material to near 0 °C, allowing the in situ reorientation of the dipolar chromophores in response to the space-charge field.

Conventionally, to apply a bias across the films, the polymer material is pressed between two transparent conductive electrodes as illustrated in Fig. 1(a). In order for excited charges to drift into the dark regions, the grating vector (oriented perpendicular to the interference fringes) must have some projection in the direction of the applied electric field. This requires the device to be tilted at an angle θ_{tilt} with respect to the bisector of the two recording beams, an angle generally of the order of 40°–50°. In a recent study, a new type of electrode configuration was implemented, and, as illustrated in Fig. 1(b), consisted of interdigitated electrodes.[5] This geometry applies the electric field within a single plane, causing it to arc upward into the bulk of the polymer, as illustrated in Fig. 1(c) maximizing the grating vector projection onto the electric-field vector. This removes the necessity of tilting the device and can enable systems that do not support the tilted geometry.

In developing these new electrodes for use with PR polymers, the electrode width and spacing are both parameters that will affect the final device performance. Larger spacing between electrodes requires the application of higher bias to reach the same electric field inside the material. Wider electrodes themselves lead to more area in which the electric field is not parallel to the grating vector. On the other hand, as these parameters decrease, the overall spatial inhomogeneity of the electric field increases. This leads to the necessity of modeling the response of the PR polymer to various electrode geometries to determine the optimal use case. PR dynamics predictions make a series of assumptions which invalidate their use in

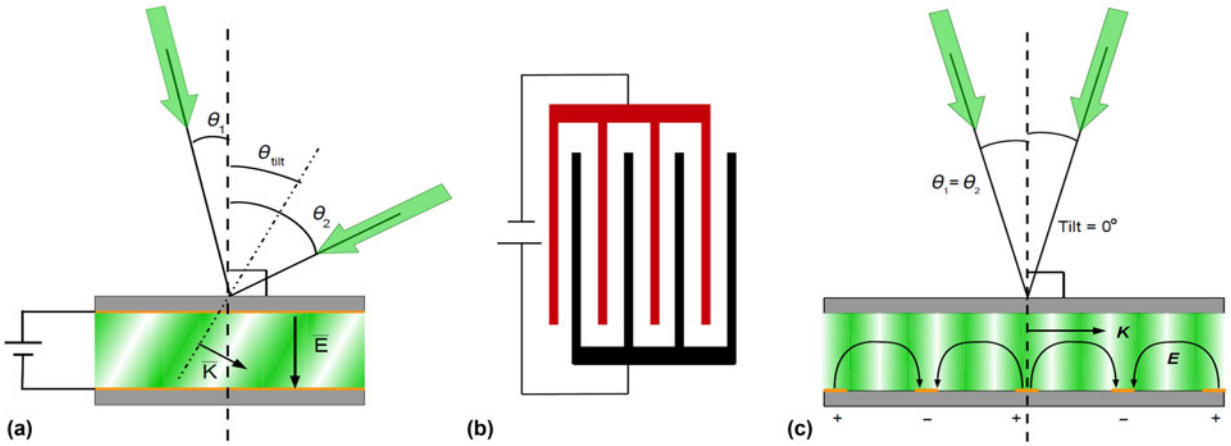

Figure 1. (a) Diagram of the electric field applied by the standard sandwich electrode configuration and the required use case for transmission hologram recording; (b) top view of the coplanar, interdigitated electrode configuration; (c) side view of the electric-field orientations and writing geometry for devices using coplanar electrodes.

low (<10 V/μm) and high (>60 V/μm) internal electric fields. In standard sandwich style electrode configuration, the use case is generally within this regime and the models are accurate predictors of the behavior. In coplanar electrode devices, the field magnitude varies greatly throughout the bulk of the polymer, with values often outside the valid use case regime, and a method of extending the current model to accurately take into account these regimes must be developed to make accurate predictions.

One of the advantages of this coplanar geometry is that it enables the direct imaging and characterization of material response to electric fields through the use of techniques such as electric-field induced second-harmonic generation (EFISHG). EFISHG is a standard optical probing technique for nonlinear optical materials and their response to external stimuli.[6] Investigation of these properties using either the standard sandwich style electrodes or a corona discharge-type geometry has been performed in previous works but these configurations limited the analysis to the bulk response of the material. This method effectively integrates both the material response and electric-field inhomogeneities throughout the thickness of the polymer film.[7–10] In this paper, coplanar electrodes in conjunction with multiphoton microscopy was used to probe in situ chromophore orientation due to spatially modulated electric fields through EFISHG. The experimental response of the chromophores in the low-field magnitude regions was used to extend the validity of the current PR model to the low fields necessary for this analysis. These results were used to adjust the electric-field-dependent parameters in predicting the effect of coplanar electrode geometry on the uniformity of PR-based holographic displays.

Electric field enhanced second-harmonic generation

EFISHG is a third-order nonlinear optical process in which one of the three input frequencies is a DC electric field.[11] This externally applied field affects the macroscopic order of the system, namely by orienting the polar chromophores and creating a bulk asymmetry, required for a second-order optical response. The nonlinear optical polarizability ($P_i^{2\omega}$) of such a system can be written

$$P_i^{2\omega} = \chi_{ijkl}^{(3)}(-2\omega;\ \omega,\ \omega,\ 0)E_j^{\omega}E_k^{\omega}E_l^{0}, \tag{1}$$

in which E_j^{ω} and E_k^{ω} are the incident optical fields of frequency ω, E_l^0 is the externally applied DC electric field, and $\chi_{ijkl}^{(3)}(-2\omega;\ \omega,\ \omega,\ 0)$ is the third-order susceptibility of the bulk system for EFISHG. In the case of PR polymers, upon the application of the external field, the dipole of the chromophore causes the molecules to rotate and partially align to the field.[12] The bulk nonlinear polarizability in this case can be rewritten in a more convenient manner with an electric-field-dependent second-order polarizability replacing the third-order polarizability as

$$\begin{aligned} P_i^{2\omega} &= \chi_{ijk}^{(2)}(-2\omega;\ \omega,\ \omega)(E^0)\ E_j^{\omega}E_k^{\omega}; \\ \chi_{ijk}^{(2)}(-2\omega;\ \omega,\ \omega)(E^0) &= \chi_{ijkl}^{(3)}(-2\omega;\ \omega,\ \omega,\ 0)E_l^0. \end{aligned} \tag{2}$$

Typical chromophores exhibit cylindrical symmetry with hyperpolarizability confined to the long axis of symmetry along which the dipole is oriented. This results in the tensor elements of the polarizability only being significant in the directions perpendicular or parallel to the poling field. As the purpose of the current study was to analyze the relative field dependence of the orientation of the chromophores subject to a spatially varying bias, only the general form of the second-order polarizability is necessary for this analysis.

The optical intensity of the generated second-harmonic [$I(2\omega)$] is related to $\chi^{(2)}$, E^0 and the incident optical power [$I(\omega)$] through

$$I(2\omega) \propto (\chi^{(2)})^2 I^2(\omega) \propto (E^0)^2 I^2(\omega). \tag{3}$$

This quadratic dependence of the generated second-harmonic optical intensity on the degree of molecular orientation translates into a similar quadratic relationship to the applied electric field.

EFISHG through multiphoton microscopy

The magnitude of the second-order susceptibility for this type of poled polymer system is relatively small, requiring high fundamental frequency intensity to produce a significant signal at the second-harmonic frequency. The system employed in these measurements was a near-IR laser-scanning microscope, described in detail by Kieu et al.[13] The fundamental illumination was provided by a 1560 nm, 190 fs pulse width, 75 MHz repetition rate fiber laser with 50 mW average power. A linear polarizer inserted into the collimated fiber laser output linearly polarizes the excitation source and results in 25 mW average power at the measurement plane. The orientation of the linear polarization was aligned with the direction of chromophore orientation using a half wave plate prior to the scan mirror. The pulses have a Gaussian shape in the time domain with an estimated peak power of 1.54 kW and energy per pulse of 0.333 nJ.[14] The microscope objective in this system was a NewFocus 0.5 NA aspheric lens, resulting in a focused beam waist of 0.609 μm. Thus, the peak power intensity was able to reach 1.06×10^{12} W/cm^2.

In this type of focusing system, the objective lens imparts polarization changes to the beam profile with respect to the incident wavefront. For investigation of poled polymer systems using EFISHG, this could lead to an axial polarization component to the observed signal. For the case of an aplanatic, well-corrected system, such as the aspheric objective used in this microscope, this effect can be quantified using a geometry-based ray-bending analysis.[15] For a 0.5 NA objective and incident x polarization, the magnitude of the electric-field vector components at the focal plane, $|E_x|^2$, $|E_y|^2$, and $|E_z|^2$ normalized to a total intensity of unity are 0.98, 7.15×10^{-5}, and 0.018, respectively. Additionally, taking into account the $I(2\omega) \propto I^2(\omega)$ relation, the y- and z-polarization contributions to these measurements are negligible.

The interdigitated electrodes were 30 nm thick ITO on glass and were lithographically fabricated with 10 μm electrode width, 100 μm inter-electrode spacing, and 5 mm finger length. The polymer composite was prepared by melt processing between the electrode and a blank glass cover slide with an active thickness of 100 μm. The second-harmonic signal (780 nm) was collected with 0.5 μm in-plane microscope resolution and in 2 μm vertical steps through the bulk of the PR polymer. Each measurement plane was parallel to the electrode plane. Figure 2 shows a log scale cross-section through the resulting volume of second-harmonic signal in false color [$\log_{10}$ (counts)] with an applied bias of 4000 V. The central 100 μm repeating structure corresponds to the region between two electrode fingers of opposite polarity with the electrodes located at the zero point on the vertical graph axis.

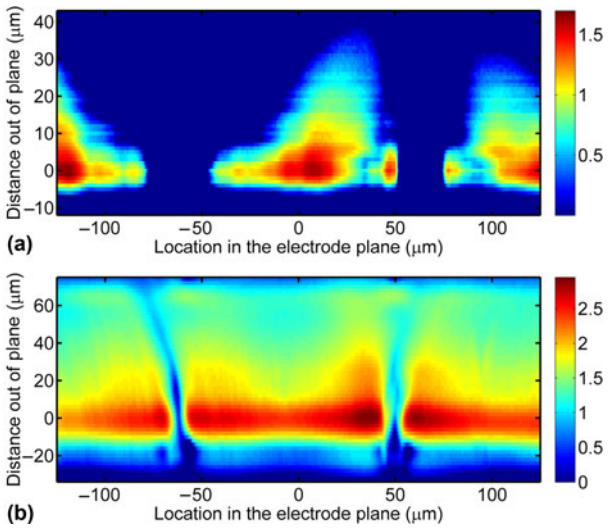

Figure 2. Cross-section of the intensity [$\log_{10}$ (counts)] of the second-harmonic signal measured through the thickness of the polymer in the case of (a) hole-conducting PATPD, 2000 V applied bias and (b) non-conductive polystyrene, 4000 V applied bias. The grounded electrode is the right electrode imaged, located ~50 μm.

Preliminary EFISHG investigations were undertaken using the standard hole conducting polymer base PATPD, with results shown in Fig. 2(a). The asymmetric form of the SHG signal is due to a decrease in electric-field magnitude near the bias electrode. This indicates the presence of photoconductivity in the device and the location near the bias electrode signifies that the mobile species are holes, as would be expected in a hole-conducting polymeric system such as this. Typically the bulk effect of photoconductivity is relatively small but in the presence of intense optical fields, this effect obscures the direct electric-field relationship to the intensity of second-harmonic signal. Subsequent characterizations were performed on a reduced conductivity system to decrease the number of assumptions that had to be made in the analysis. The polymer composite used in the final EFISHG characterizations [see sample measurement in Fig. 2(b)] was composed of the non-conductive polymer polystyrene, ECZ and 7-DCST in the weight percent ratio of 55:20:25. The polystyrene composite was comparable with that of the standard PATPD-based formulation in glass transition temperature (measured by differential scanning calorimetry) and chromophore orientation speed and magnitude (characterized by transmission ellipsometry), ensuring that the EFISHG results would be applicable to the PATPD PR uniformity analysis.

Measurements were taken over a range of applied electric fields from 0 to 4000 V and were confined to the central lengthwise region of the electrodes, far from the ends. Analysis along the length of the electrodes verifies that the orientational response is uniform in that direction in this measurement area. The intensity of the second-harmonic signal taken in the plane of the electrode (0,0) is shown in Fig. 3. Based on the

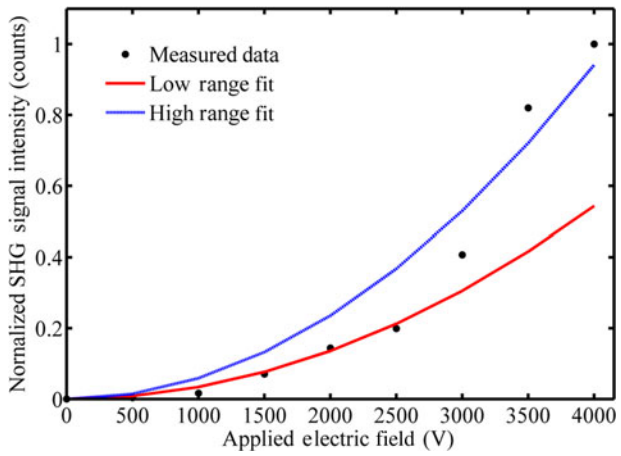

Figure 3. Intensity of the second-harmonic signal as a function of applied electric field. Low range fit is for applied electric fields <2500 V, while the high range fit is for the >2500 V range.

quadratic relation between the SHG signal and applied field, all of the data points would be expected to lie on the same E^{0^2} curve. The results, however, indicate the existence of an effective orientational barrier between 2500 and 3000 V, below which the applied field was not high enough to fully overcome the thermal reorientation of the chromophores. The SHG intensity versus applied electric field was fit to $I(2\omega) = C \times (E^0)^2$ for the low- and high-field cases with the resulting trends shown in Fig. 3. Above 3000 V applied bias, the standard chromophore orientation response to the electric field in the PR response models was valid. As indicated by the results at low bias, an orientational threshold voltage exists for the system under test and a modification to the following model was necessary for the regions of the device with lower field magnitudes.

Diffraction uniformity model

A map of the electric field was calculated for the experimental coplanar electrode geometry for use in the PR model to predict diffraction uniformity. By assuming an infinite extent of the electrodes along their length, this 3D geometry can be reduced to a two-dimensional (2D) analysis, producing the applied electric fields and orientation in the PR material with minimal computation time. This assumption is valid due to the configuration of our electrodes, with the length 50 times larger than the electrode width and spacing and the illumination occurring well away from the ends of the electrodes. The Laplace equation, $\nabla^2 V = 0$, describes the electrostatic potential in a nonconductive media according to Dirichlet boundary conditions which set the applied bias at the electrodes, and Newmann conditions which constrain the form of the response along the remaining boundaries.

The response of the polymer system to an external bias depends on the overall magnitude of the electric field [Fig. 4(a)] in some cases; in others it is the projection of the electric-field vector onto the grating vector that is the dominant factor. Figure 4(b) shows the calculated electric-field projection onto a horizontal grating vector resulting from an untilted geometry. Figure 4(c) displays the comparison of the theoretical horizontal projection of the applied electric field and the square-root of the EFISHG values $[I(2\omega) \propto (E^0)^2]$ in the plane of the electrode ($z = 0$) at 4000 V applied bias. Since the EFISHG measurements are qualitative in nature for this application, the measurement was normalized to the central field value for the model. It can be seen that there is a good degree of agreement between the electric-field model and the measurement which means that upon taking into account the low-field orientation correction factor, this electric-field model can be used for predicting PR response to coplanar electrodes. The decreased peak intensity of the SHG signal at the edges of the range seen in Fig. 4(c) is due to the slightly curved focal plane of the scanning beam across the extent of the image plane. The central electrode region spanning from −55 to +55 μm in Fig. 4 is the section over which the generated signal that was collected originates from the same 2 μm vertical measurement step. Outside this range, the focal location of the fundamental beam is higher, reducing the peak intensity with which the second harmonic was generated. Owing to this, the central electrode region is the one that is used for measurement analysis, such as in Fig. 3.

Dynamic models of photorefractivity in polymers have long been used to direct the formulation of new and more efficient PR devices. Ostroverkhova modified the Schildkraut and Buettner model describing the relationship between material parameters and electric fields and their contribution to the PR response.[16–18] The response depends on a variety of material parameters such as sensitizer densities and trap levels, but in this case the focus is on the effect of the electric-field-dependent parameters. These are the photogeneration cross-section (s), hole drift mobility (μ), and trapping (γ) and recombination (γ_T) rates with field dependencies on either the magnitude of the applied field or the projection of the field onto the grating vector. The calculation parameters for this analysis were set to match the subsequent test cases, with angle of 30° between the two writing beams, tilt angles ranging from 0° to 20° with respect to the sample normal (effectively changing the orientation of the grating vector with respect to the sample normal), a recording wavelength of 532 nm, and illumination of 30 mW/cm^2. Using the electric-field model to evaluate these parameters across the electrodes, and incorporating the low-field adjustments from EFISHG measurements, the resulting space-charge field was used to calculate the refractive index modulation of the form

$$\Delta n = \text{constant} \times E^0 \times |E_{sc}| \times \cos\,\varphi, \qquad (4)$$

where φ is the angle between the grating vector and the electric-field vector. The constant term is related to material parameters and is not field dependent. The orientational corrections to the electric field from Fig. 3 decrease the low applied field contribution to the index modulation.

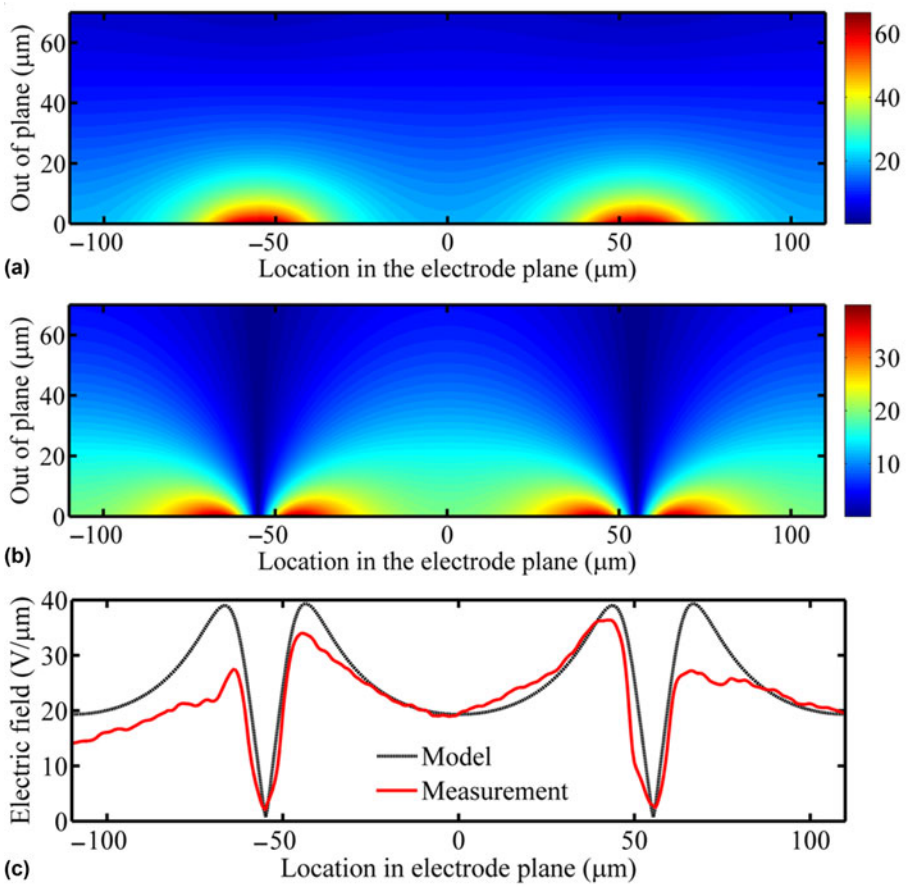

Figure 4. (a) Electric-field magnitude and (b) horizontal vector component applied by coplanar electrodes at 4000 V bias. Electrode width 10 μm, spacing between electrodes 100 μm, magnitude units in V/μm; (c) comparison of theoretical horizontal electric-field component at the electrode surface ($z = 0$) with the value obtained from EFISHG measurements at 4000 V applied bias.

The index modulation calculated here results in the diffraction grating that is recorded in response to the interference of the writing beams in the material, so the decrease in electric field with increasing distance from the electrodes [Figs. 4(a) and 4(b)] and subsequent refractive index modulation that is an order of magnitude higher near the edges of the electrodes than in the remaining bulk of the material affects the diffraction of the reading beam. Computational propagation of the reconstructed beam through the grating to analyze diffraction uniformity across the beam was performed using the Crank–Nicholson method.[19] Implementation of periodic boundary conditions took advantage of the repeating nature of the electrode structure, so only three repeating electrode structures were used along with a device thickness of 100 μm. Solution verification was performed by calculating the diffraction grating due to a uniform electric field under the same writing conditions and propagating both planar and Gaussian wavefront optical fields through it. Both incident field results showed the expected 100% uniformity of the diffracted beam. These tests additionally validated the use of an infinite extent plane wave in the following analysis to remove the Gaussian envelope from the uniformity analysis.

Figure 5(a) shows the results of the spatial distribution of the diffracted beam after propagation through the PR polymer across one period of the electrode structure. The effect of the spatially inhomogeneous electric fields is to concentrate diffraction of the reconstructed beam near the electrode edges, which affects the resulting beam uniformity in a high spatial frequency manner. Tilting the writing beams with respect to the normal to the sample plane increases the number of these high index regions that the reconstruction beam encounters. For a range of tilt angles from 0° to 20°, the high-frequency components peak power to root-mean-squared (RMS) ratio decreases by 15%. Also called the crest factor in signal processing, the peak to RMS ratio is a measure of how extreme the peaks are in a signal, and indicates an increase in the spatial homogeneity of the reconstructed beam with increasing tilt angle.

To analyze the low spatial frequency effects of diffraction from the underlying electrode structure, an 800 μm diameter Gaussian beam was propagated through basic split-step beam propagation and absorbing boundary conditions with a 40 mm analysis space. The grating parameters and thickness remained the same with respect to the previous model. The

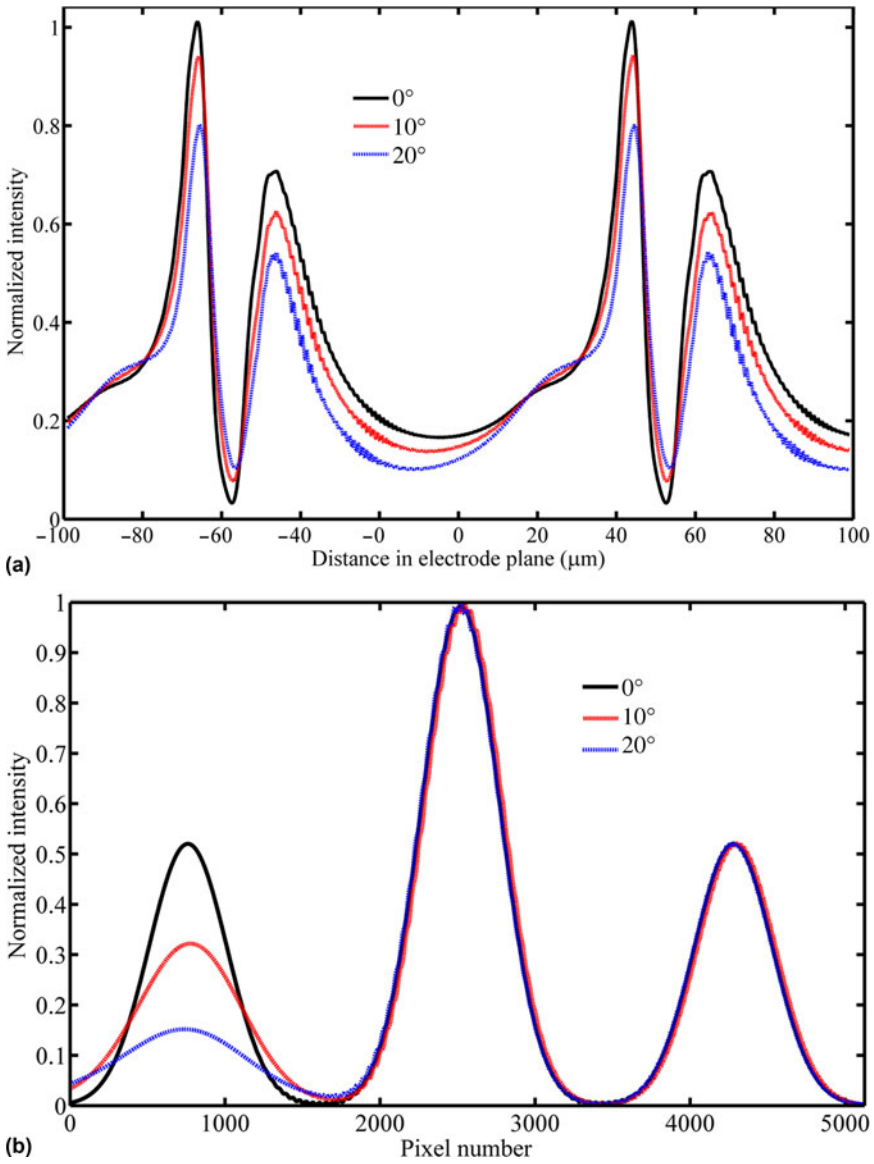

Figure 5. Propagated reconstructed beam at 0°, 10°, and 20° degree tilt angle geometries of the recording beams in (a) electrode and (b) full beam scales.

change in the analysis method used here was due to the increased robustness of this propagator at larger sampling steps (to counter the larger analysis space in computation time), which, while obscuring some of the fine detail represented in Fig. 5(a), reproduced the lower spatial frequency results accurately. Figure 5(b) shows the propagation results of the full width of the reading beam in the output plane (total diffracted angle 30°). The central portion is the primary diffracted beam from the high-frequency grating and is Bragg matched to that grating. The presence of side lobes is due to diffraction from the underlying low spatial frequency refractive index modulation from the periodicity of the applied electric field. The angle of diffraction from this grating period is only ~0.09° and both of the side lobes deviate slightly from the Bragg angle of the high-frequency grating, reducing the efficiency of their diffraction. With increasing tilt angle, the diffracted order that is closer to the sample normal than the reconstructed Bragg angle (left peak) is less efficiently diffracted by the base structure due to its increasing Bragg mismatch.

Model validation through non-degenerate four-wave mixing

Experimental verification of the applicability of these adjusted models in device design was executed. Non-degenerate four-wave mixing measurements were performed in which a grating was formed by two TE polarized 532 nm mutually coherent beams with an inter-beam angle of 30°. The orientation of the coplanar electrodes was also such that the electrodes

extended in the TE direction, ensuring that the generated charges traveled across the fringes to become trapped instead of along them. A 633 nm reading beam counter-propagating at the appropriate angle accounting for the wavelength mismatch diffracted from the grating and was monitored by a CMOS detector for 0°, 10°, and 20° tilt angles. Figure 6(a) shows the original and diffracted beam profiles taken in a cross-section perpendicular to the plane of diffraction. As expected, there was no significant change in the profile of the beam since this is the direction along the fringes and perpendicular to the underlying electrode index modulation. Figure 6(b) is a cross-section in the plane of the electrode index modulation and multiple orders flanking the primary diffracted beam are present. Note that the original beam intensity was scaled to the range of the central diffracted lobes. Variability between the intensity of the central lobes for the different tilt angles is due to minor alignment deviations between the configurations but normalization of these results would have unduly emphasized the fine structure of some of the measurements. The decrease in the intensity of the left order follows that of the theoretical model [Fig. 5(b)]. The fine structure inhomogeneity from the micron-scale diffraction analysis is seen in the side lobes orders but is insignificant with respect to the magnitude of the full diffracted beam. This indicates that the non-uniformity due to the spatial electric-field modulation is a more significant effect on the secondary orders.

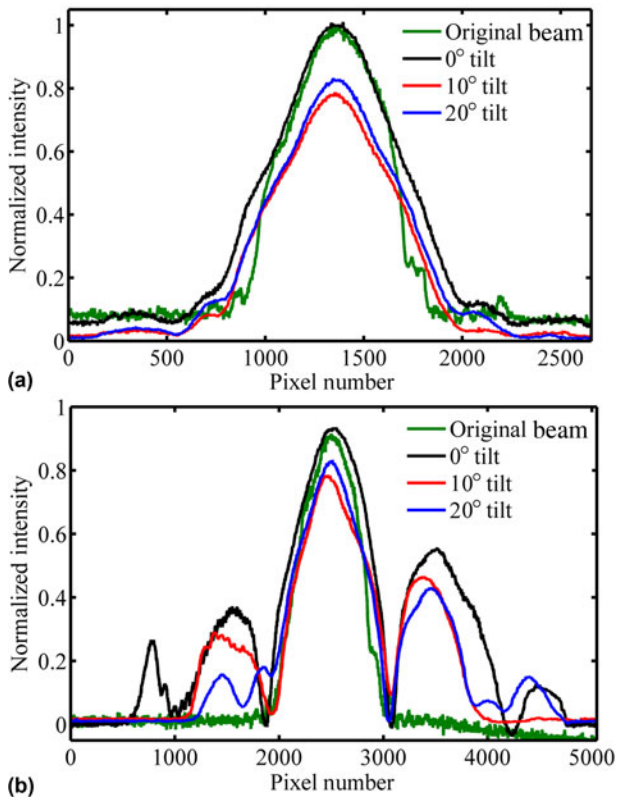

Figure 6. Cross-sections of the measured incident and diffracted beam profiles taken (a) out of the plane of diffraction and (b) in the plane of diffraction for various tilt angles.

Conclusions

Interdigitated electrodes are a novel electrode configuration for use in PR polymer devices that enables diffraction without applying tilt in the recording geometry. This pattern, however, generates a highly inhomogeneous electric field within the bulk of the material that impacts the diffraction amplitude and uniformity. In this paper, the EFISHG technique was used to directly image the orientation of the chromophores to the electric field. The observed response was used to adjust the standard model of refractive index modulation in PR polymer devices to take into account the non-uniform electric fields. The corrected PR response model was used to calculate the recorded holographic gratings and enabled predictions of diffraction uniformity across the beam through computational wavefront propagation. Observations of diffracted beam uniformity correlate to the model predictions, indicating that this model is valid in predicting the effect of the coplanar geometries, including the extreme field magnitude regions.

Future work will include using this validated model to optimize the electrode parameters for maximum diffraction uniformity. These devices will then be fabricated for further testing and characterization. Additionally, the EFISHG technique may be used in studies of new conductive polymers for PR application as it was seen to afford an in situ qualitative measure of conductivity. In dispersive transport systems such as PR polymers where time-of-flight measurements are inconclusive for measuring mobilities, this technique may yet provide an alternative measurement method.

Acknowledgments

The authors acknowledge support from the DoD SMART Scholarship program, TRIF support through the State of Arizona, AFOSR contract FA9550-10-1-0207, and the National Science Foundation through CIAN NSF ERC under grant #EEC-0812072. Additionally, they would like to thank undergraduate researchers Alan Yeh and Maryam Tanbal from the University of Arizona and Joshua Miller from the University of Albany for their assistance.

References

1. S. Ducharme, J.C. Scott, R.J. Twieg, and W.E. Moerner: Observation of the photorefractive effect in a polymer. *Phys. Rev. Lett.* **66**, 1846 (1991).
2. K. Meerholz, B.L. Volodin, Sandalphon, B. Kippelen, and N. Peyghambarian: A photorefractive polymer with high optical gain and diffraction efficiency near 100%. *Nature* **371**, 497 (1994).
3. M. Eralp, J. Thomas, G. Li, S. Tay, A. Schulzgen, R.A. Norwood, N. Peyghambarian, and M. Yamamoto: Photorefractive polymer device with video-rate response time operating at low voltages. *Opt. Lett.* **31**, 1408 (2006).
4. P.-A. Blanche, A. Bablumian, R. Voorakaranam, C.W. Christenson, W. Lin, T. Gu, D. Flores, P. Wang, W.-Y. Hsieh, M. Kathaperumal, B. Rachwal, O. Siddiqui, J. Thomas, R.A. Norwood, M. Yamamoto, and N. Peyghambarian: Holographic three-dimensional telepresence using large-area photorefractive polymer. *Nature* **468**, 80 (2010).

5. C.W. Christenson, C. Greenlee, B. Lynn, J. Thomas, P.-A. Blanche, R. Voorakaranam, P. St. Hilaire, L. Lacomb Jr., R.A. Norwood, M. Yamamoto, and N. Peyghambarian: Interdigitated coplanar electrodes for enhanced sensitivity in a photorefractive polymer. *Opt. Lett.* **36**, 3377 (2011).
6. Ch. Bosshard, J. Hulliger, M. Florsheimer, and P. Gunter: *Organic Nonlinear Optical Materials* (CRC Press, London, England, 2001).
7. K.D. Singer, M.G. Kuzyk, W.R. Holland, J.E. Sohn, S.J. Lalama, R.B. Comizzoli, H.E. Katz, and M.L. Schilling: Electro-optic phase modulation and optical second-harmonic generation in corona-poled polymer films. *Appl. Phys. Lett.* **53**, 1800 (1988).
8. O. Ostroverkhova, A. Stickrath, and K.D. Singer: Electric field-induced second harmonic generation studies of chromophore orientational dynamics in photorefractive polymers. *J. Appl. Phys.* **91**, 9481 (2002).
9. G. Lüpke, C. Meyer, C. Ohlhoff, H. Kurz, S. Lehmann, and G. Marowsky: Optical second-harmonic generation as a probe of electric-field-induced perturbation of centrosymmetric media. *Opt. Lett.* **20**, 1997 (1995).
10. A.V. Vannikov, Y.G. Gorbunova, A.D. Grishina, and A.Y. Tsivadze: Photoelectric, nonlinear optical, and photorefractive properties of polymer composites based on supramolecular ensembles of Ru(II) and Ga (III) complexes with tetra-15-crown-5-phthalocyanine. *Prot. Met. Phys. Chem. Surf.* **49**, 57 (2013).
11. R.W. Boyd: *Nonlinear Optics*, 3rd ed. (Elsevier Science, Philadelphia, 2008).
12. L.R. Dalton, A.W. Harper, and B.H. Robinson: The role of London forces in defining noncentrosymmetric order of high dipole moment-high hyperpolarizability chromophores in electrically poled polymeric thin films. *Proc. Natl. Acad. Sci. USA* **94**, 4842 (1997).
13. K. Kieu, S. Mehravar, R. Gowda, R.A. Norwood, and N. Peyghambarian: Label-free multi-photon imaging using a compact femtosecond fiber laser mode-locked by carbon nanotube saturable absorber. *Biomed. Opt. Express* **4**, 334 (2013).
14. K. Kieu and M. Mansuripur: Femtosecond laser pulse generation with a fiber taper embedded in carbon nanotube /polymer composite. *Opt. Lett.* **32**, 2242 (2007).
15. M. Mansuripur: *Classical Optics and its Application*, 2nd ed. (Cambridge University Press, Cambridge, England, 2009).
16. O. Ostroverkhova and K.D. Singer: Space-charge dynamics in photorefractive polymers. *J. Appl. Phys.*, **92**, 1727 (2002).
17. J.S. Schildkraut and Y. Cui: Zero-order and first-order theory of the formation of space-charge gratings in photoconductive polymers. *J. Appl. Phys.* **72**, 5055 (1992).
18. J.S. Schildkraut and A.V. Buettner: Theory and simulation of the formation and erasure of space-charge gratings in photoconductive polymers. *J. Appl. Phys* **72**, 1888 (1992).
19. W.H. Press, S.A. Teukolsky, W.T. Vetterling, and B.P. Flannery: *Numerical Recipes 3rd Edition: The Art of Scientific Computing*, 3rd ed. (Cambridge University Press, Cambridge, England, 2007).